SCIENTIFIC REPORTS
nature research

OPEN

LiB_{13}: A New Member of Tetrahedral-Typed B_{13} Ligand Half-Surround Cluster

Hongxiao Shi[1], Xiaoyu Kuang[1*] & Cheng Lu[2*]

It will get entirely unusual derivatives with gratifying chemical bonding schemes for boron clusters by doping with lithium, the lightest alkalis. The geometric structures and electronic properties of the $LiB_n^{0/-}$ ($n = 10-20$) clusters have been studied through Crystal structure AnaLYsis by Particle Swarm Optimization (CALYPSO) structural search approach along with the density functional theory (DFT) calculations. The low-lying candidates of $LiB_n^{0/-}$ ($n = 10–20$) are reoptimized at the B3LYP functional in conjunction with 6–311 + G(d) basis set. Three forms of geometric configurations are identified for the ground-state structures of $LiB_n^{0/-}$ clusters: half-sandwich-type, quasi-planar and drum-type structures. The photoelectron spectra (PES) of the LiB_n^- clusters have been calculated through time-dependent density functional theory (TD-DFT). A promising LiB_{13} with tetrahedral-typed B_{13} ligand half-surround cluster and robust stability is uncovered. The molecular orbital and adaptive natural density partitioning (AdNDP) analysis show that B-B bonds in the B_{13} moiety combined with the interaction between the B_{13} shell and Li atom stabilize the C_{2v} LiB_{13} cluster. Our results advance the fundamental understanding about the alkali metal doped boron clusters.

It is a significant milestone in the nanomaterials science that Kroto *et al*. discovered the C_{60} fullerene[1], which aroused a surge of research activities about carbon. As the neighbor of carbon, boron has aroused much research[2–8] because of its potential application and electron deficiency[9,10]. B_{40}[11], the boron analogue of C_{60}, has also been experimentally observed[12]. Researches over the past few years manifested that the lowest-energy structures of the $B_n^{-/0/+}$ clusters tend to be planar\quasi-planar. Detailly, the ground-state structures of the B_n^- clusters keep to be planar\quasi-planar till $n = 36$ (B_{36}^-)[13–15], $n = 20$ for the B_n clusters[16] and $n = 16$ for the B_n^+ clusters[17]. Soon after, the evolution from planar to fullerene-like structures, B_{39}^-[18], for the B_n^- clusters appeared when n approximately equal to 40. For the positive one, the cage-like structure which can be seen as a new borospherene contains 39 boron atoms[19].

It will open a new chapter for boron clusters by doping with metal atom, which can get entirely unusual derivatives with gratifying chemical bonding schemes. In the last few years, there were great deals of reports about transition-metal-doped (TM-doped) boron clusters. These studies indicate that the configurations of the TM-doped boron clusters are contrast to that of pure boron clusters. TM-centered boron rings, $Co@B_8^-$, $V@B_9^-$, $Nb@B_9^-$, $Ta@B_9^-$, $Ru@B_9^-$, $Ta@B_{10}^-$[20–22], have been experimentally observed. Subsequently, the Co-centered drum-type structure of CoB_{16}^- cluster[23] and the half-sandwich-type structure of $Co/Ru/IrB_{12}^-$ cluster[24,25] have been found by Wang and coworkers. In addition, RhB_{18}^- cluster[26] has been found that there are two different configurations for the ground state and both of the structures have been observed experimentally. In the year of 2017, a unique tubular molecular rotor has been observed for the global minimum of the TaB_{20}^- cluster[27]. The $MnB_n^{-/0/+}$ ($n = 10-20$) clusters have been systematically studied to reveal the geometric constructions of middle-sized boron clusters after doping of a manganese atom[28]. Not only the transition metals, other metallic elements also have been used as dopants. The $Al_2^+[B_7^{3-}]$ and $Al^+[B_8^{2-}]$[29] clusters, both of which are umbrella-type structures, have been observed through experimental and theoretical studies. PrB_7^-, a rare-earth-atom-doped boron cluster, has been researched through photoelectron spectroscopy[30]. Doping of alkali metal atom into B_3^- cluster, which can get stable $AM^+[B_3^-]$ (AM = Li-Cs) cluster, has been theoretically predicted[31]. In addition, Alexandrova and coworkers[32] found a stable C_{2v} LiB_6^- cluster using the *ab initio* study. There is also a theoretical studies of the small-sized LiB_n ($n = 1–8$) cluster[33].

[1]Institute of Atomic and Molecular Physics, Sichuan University, Chengdu, 610065, China. [2]School of Mathematics and Physics, China University of Geosciences (Wuhan), Wuhan, 430074, China. *email: scu_kuang@163.com; lucheng@calypso.cn

Although there are some studies about the Li-doped boron clusters, all the previous investigations are almost small-sized clusters except for LiB_{12}[34] and LiB_{20}[35]. It is of crucial importance for us to have a systematical study of middle-sized Li-doped boron clusters. Here, extensive structure searches of the LiB_n cluster were carried out using the CALYPSO structural search method. Subsequently, the predicted structures were reoptimized through the DFT calculations. Furthermore, we discussed the inherent stabilities of the lowest-energy structures of the LiB_n clusters. Moreover, the theoretical PES of the ground-state anionic structures had been simulated. To interpret the stabilization mechanism, chemical bonding analyses were carried out.

Results and Discussions

Geometrical structures. The calculated low-lying isomers of neutral and anionic LiB_n ($n = 10$–20) clusters are exhibited in Figs. 1 and 2, respectively. Each isomers of the cluster is denoted by the labels: $na^{/-}$, $nb^{/-}$ or $nc^{/-}$. In brief, n is the number of B atoms of the corresponding cluster; a, b, c indicates the ground-state structure and the metastable structure, alphabetically. Beside the label, there is also the point group symmetry and relative energy (eV) of the corresponding structure. (The corresponding lateral views of the low-lying isomers are shown in Figs. S1 and S2 in the Supplementary Information.) As presented in Figs. 1 and 2, most of the structures, when $n \leq 15$, grasp high point group symmetry. The lowest-energy structures of the $LiB_n^{0/-}$ ($10 \leq n \leq 15$) clusters present in forms of half-sandwich type, while for $n \geq 16$ turn out to be quasi-planar and drum-type structures. Both the anionic and neutral ground-state structures of LiB_{10}–LiB_{15}, except for LiB_{11}, are presented as half-surrounded structures, where the B_n moiety half surround to the Li atom. For the a/a$^-$ structure of the LiB_{10} cluster, the B_{10} shell is a quasi-plan with two inner B atoms surround by an outer B_8 ring. As exceptions, the structures of $LiB_{11}^{0/-}$ are plane structures. For the rest half-sandwich-type structures, the B_n fragments of 12a/a$^-$ and 14a are more flat than that of 13a/a$^-$, 14a$^-$ and15a/a$^-$. It should be noteworthy that the B_{13} ligand of the 13a/a$^-$ is no longer planar or quasi-planar but a tetrahedral-typed structure, which is in stark contrast to that of pure B_{13} cluster[36] through doping of a Li atom. All of the 16a/a$^-$, 17a/a$^-$ and 19a have a pattern that a quasi-planar B_n moiety with a doped Li atom connected to it, showing a quasi-planar structure. 19a$^-$ possesses an intermediate structure of quasi-planar and half-sandwich-type. Both the 20a and 20a$^-$ are beautiful drum-type structures. However, there are some distinctions between the structure of 18a/a$^-$ and 20a/a$^-$ where the Li atom is outside of the B_{18} drum. It is worth noting that the acquisition of an electron has little influence on the lowest-energy structures of $LiB_n^{0/-}$ clusters except for LiB_{13} and LiB_{19}. Diversely, there are some changes for the low-lying isomers due to the acquisition of an electron.

Photoelectron spectra. To deeply understanding the electronic structures of LiB_n cluster, the simulated PES of LiB_n^- ($n = 10$–20) clusters are displayed in Fig. 3. The calculated PES together with the laboratorial PES of LiB_6^- cluster[32], a smaller species than our LiB_n cluster, are displayed in Fig. S3 in the Supplementary Information. For each spectrum, the location of the first peak (X peak) indicates the vertical detachment energy (VDE), which denotes electronic detachment transition from the ground-state anion to the corresponding ground-state or excited-state neutrals. The VDE values of the LiB_n^- clusters are presented in Table S1 in Supplementary Information. The calculated spectrum of LiB_{10}^- is sparse and the VDE is about 2.29 eV. Inversely, the spectrum of LiB_{11}^- expresses a compact spectral pattern except for the X peak, which located at 1.47 eV. There are four major peaks of the LiB_{12}^- PES and the VDE is about 2.48 eV, which corresponding to the position of the first peak. For LiB_{13}^-, there are five peaks and the VDE value is 2.44 eV. For the theoretical spectrum of LiB_{14}^-, the X Peak and A peak are very similar in shape and the X peak is located about 3.06 eV. The spectral pattern of LiB_{15}^- PES is crowded, of which the VDE value is 2.84 eV. There are five peaks of the LiB_{16}^- PES, of which the VED is 3.18 eV. The PES of LiB_{17}^- is compact and the value of VDE is about 2.76 eV. There are five peaks of the PES of LiB_{18}^- and the first peak is located at 2.73 eV. The VDE of LiB_{19}^- is 2.37 eV and the X peak is far from the other three peaks. There are four sharp peaks in the sparse PES of LiB_{20}^-, of which the VDE value is 2.50 eV.

Relative stabilities. In our recent work, the inherent stabilities of the $LiB_n^{0/-}$ clusters are determined by three criteria: average binding energy (E_b), second-order differences of energy (Δ^2E) and the energy gap (E_{gap}). First, the E_b of $LiB_n^{0/-}$ clusters are calculated according to the following formulas:

$$E_b(LiB_n) = [nE(B) + E(Li) - E(LiB_n)]/(n+1) \quad (1)$$

$$E_b(LiB_n^-) = [nE(B) + E(Li^-) - E(LiB_n^-)]/(n+1) \quad (2)$$

Among these, E express the energy of the matching atom or cluster. The values of E_b of the ground-state clusters are presented in Table 1 and visualized in Fig. 4(a). Larger E_b value is the representation of a stronger chemical stability. The anions LiB_n clusters are more inert than the neutral ones for that the neutral E_b curve sits below the anionic curve. It is obviously that both the anionic and neutral curves roughly increase with augmentation of the cluster size n, indicating that it is easier for the formation of the larger cluster. It is worth noting that, there is a distinct heave in the neutral curve when $n = 11$.

As a sensitive argument to reflect the relative stability, the Δ^2E of the lowest-energy $LiB_n^{0/-}$ clusters is defined as:

$$\Delta^2E(LiB_n) = E(LiB_{n-1}) + E(LiB_{n+1}) - 2E(LiB_n) \quad (3)$$

$$\Delta^2E(LiB_n^-) = E(LiB_{n-1}^-) + E(LiB_{n+1}^-) - 2E(LiB_n^-) \quad (4)$$

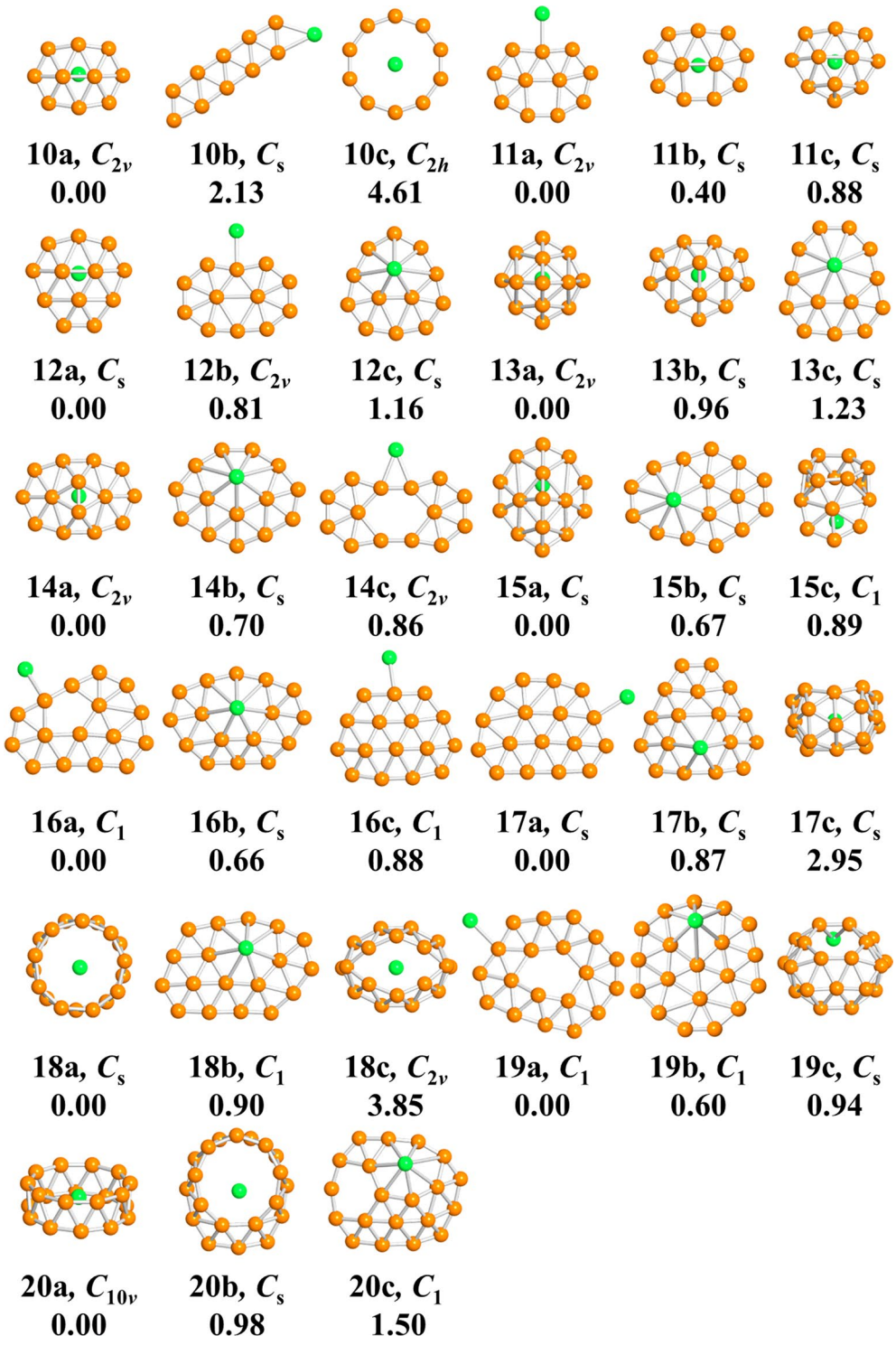

Figure 1. Optimized structures for LiB_n clusters. "na", "nb" and "nc" indicates structures alphabetically. Point group symmetry along with the relative energy (eV) is also labeled under the structures.

Both the neutral and anionic Δ^2E values can be fined in Fig. 4(b). Fig. 4(b) presents that the LiB_{11}, LiB_{13}, and LiB_{17} clusters along with the LiB_{12}^-, LiB_{14}^-, LiB_{16}^- and LiB_{18}^- clusters possess obviously higher Δ^2E values which indicating their enhanced stability relative to the immediate neighbors.

The E_{gap} between the highest occupied molecular orbital (HOMO) and the lowest unoccupied molecular orbital (LUMO) is also a signature of the stability of the corresponding cluster. The higher E_{gap} values the stronger chemical stability of the given cluster. The calculated E_{gap} values of the lowest-energy $LiB_n^{0/-}$ clusters are presented in Table 1 and Fig. 4(c). It is distinct to notice that both of the E_{gap} curves express the even-odd oscillation behavior. There are two obvious outliers for LiB_{11} and LiB_{13} cluster suggesting that they are more inert than the others.

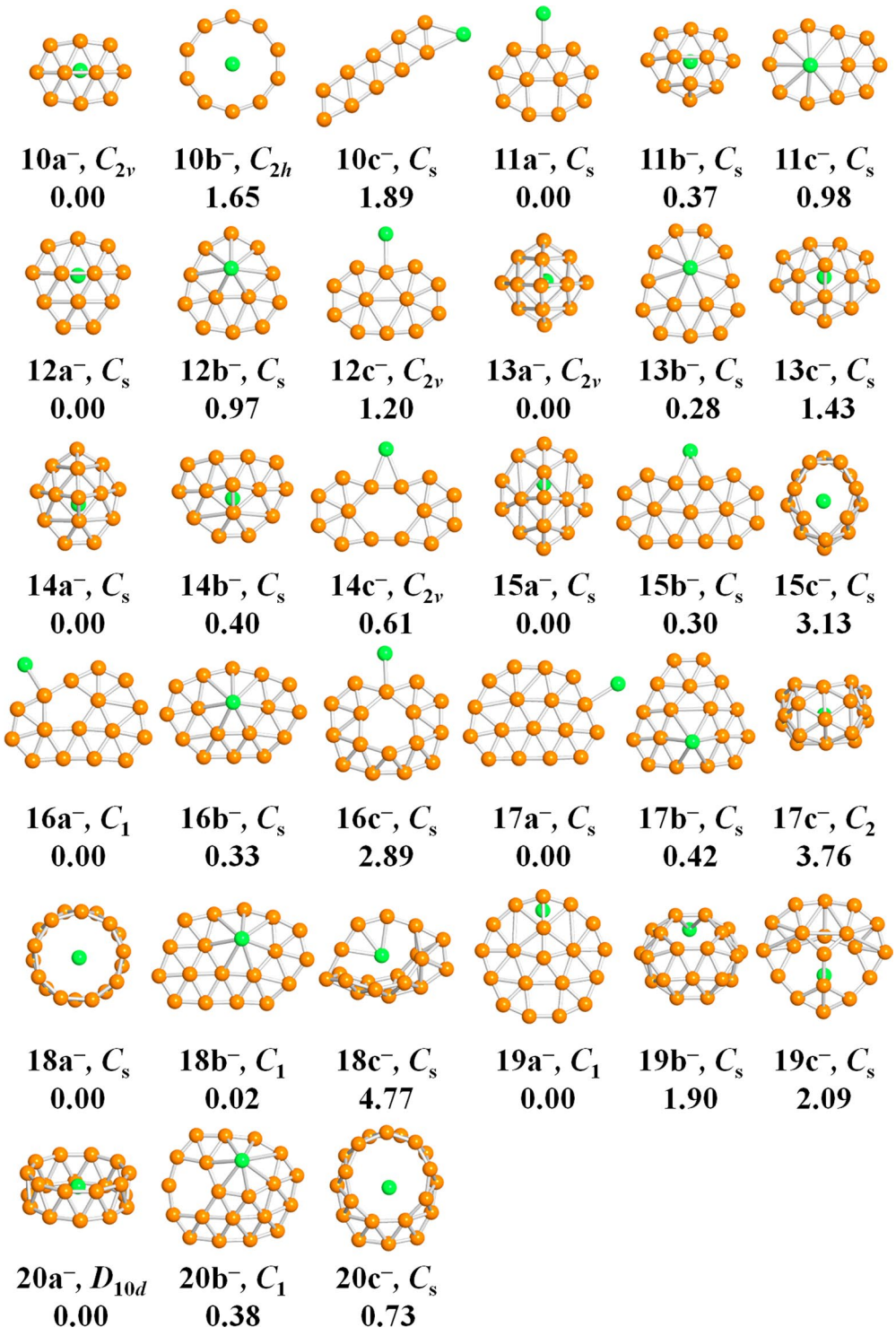

Figure 2. Optimized structures for LiB_n^- clusters. "na⁻", "nb⁻" and "nc⁻" indicates structures alphabetically. Point group symmetry along with the relative energy (eV) is also labeled under the structures.

Accordingly, we can determine that, from the results of E_b, Δ^2E, and E_{gap} above, the neutral LiB_{11} and LiB_{13} cluster can be viewed as "magic" clusters which are chemically inert.

Chemical bonding analysis. The molecular orbital (MO) and AdNDP analyses are presented to fully grasp the bonding mechanism of lithium-doped boron clusters. LiB_{13} (a half-sandwich-type structure, C_{2v}) is chosen as a representation for its chemical stability and unusual geometric structure. There are eleven pictorial MOs near the HOMO of LiB_{13} along with their corresponding energy levels in Fig. 5. The LUMO of LiB_{13} cluster is a σ-hybrid orbital and primarily formed of 2p atomic orbital (AO) of boron atom. For the rest MO of LiB_{13}, the

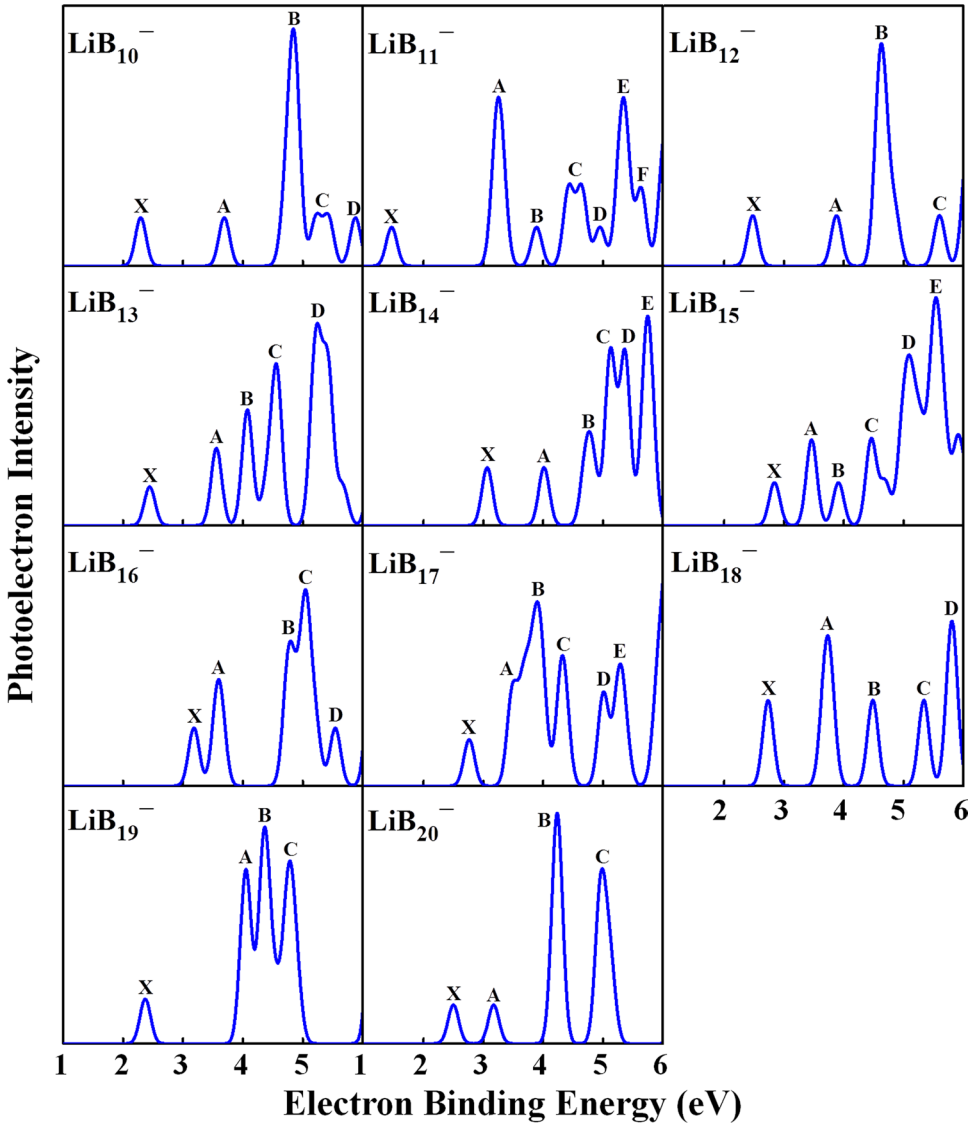

Figure 3. Calculated PES of the lowest-energy LiB_n^- (10–20) clusters.

	LiB_n				LiB_n^-			
n	Sta.	Sym.	E_b	E_{gap}	Sta.	Sym.	E_b	E_{gap}
10	$^2A_2$	C_{2v}	4.39	1.84	$^1A_1$	C_{2v}	4.54	1.93
11	$^1A_1$	C_{2v}	4.49	2.92	$^2A''$	C_s	4.56	0.72
12	$^2A'$	C_s	4.48	1.63	$^1A'$	C_s	4.61	1.93
13	$^1A_1$	C_{2v}	4.52	3.58	$^2A_1$	C_{2v}	4.63	1.43
14	$^2A_2$	C_{2v}	4.54	1.46	$^1A'$	C_s	4.68	1.98
15	$^1A'$	C_s	4.57	2.45	$^2A'$	C_s	4.70	1.08
16	^2A	C_1	4.61	1.45	^1A	C_1	4.76	2.27
17	$^1A'$	C_s	4.68	1.76	$^2A''$	C_s	4.80	1.43
18	$^2A''$	C_s	4.70	1.21	$^1A'$	C_s	4.81	1.84
19	^1A	C_1	4.68	2.07	^2A	C_1	4.81	1.35
20	^2A	C_{10v}	4.76	1.04	^1A	D_{10d}	4.85	1.43

Table 1. The calculated electronic states, symmetries, E_b (eV) and E_{gap} (eV) of ground-state $LiB_n^{0/-}$ clusters.

nondegenerate HOMO, HOMO-8 and HOMO-9 orbital, which formed by p-type AO of B atom and s-type AO of Li atom, are σ orbital. However, as σ orbital, HOMO-1 is predominantly composed by B p-orbital of the B_{13} atoms moiety. The HOMO-a (a = 2–7) feature π orbital are primarily *p*-type AOs of the B atom. Based on the

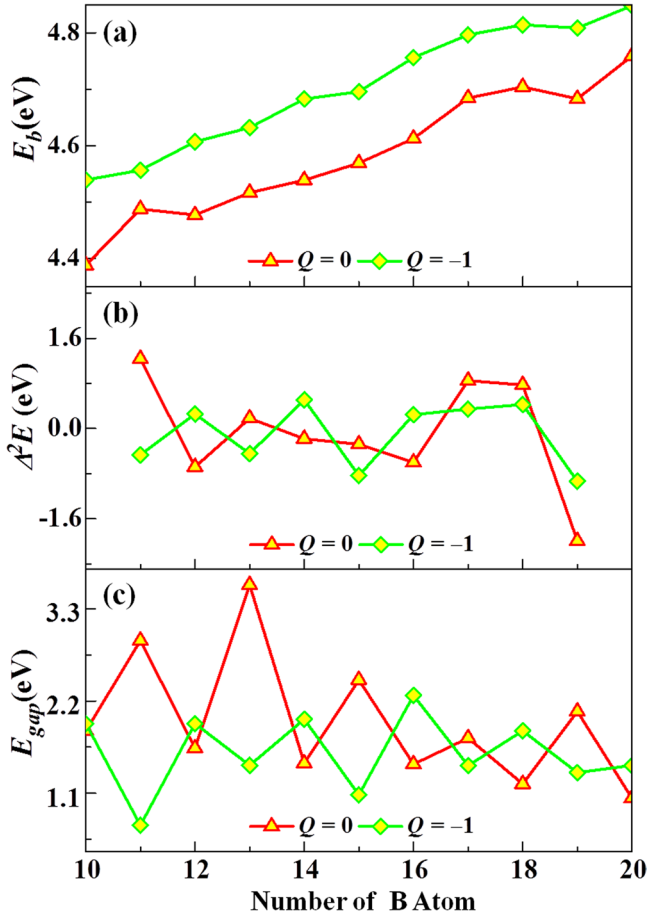

Figure 4. The (**a**) averaged binding energies (E_b, eV), (**b**) second-order energy differences (Δ^2E, eV) and (**c**) HOMO–LUMO energy gaps (E_{gap}, eV) of the ground-state LiB_n^Q (n = 10–20, Q = 0, −1) clusters.

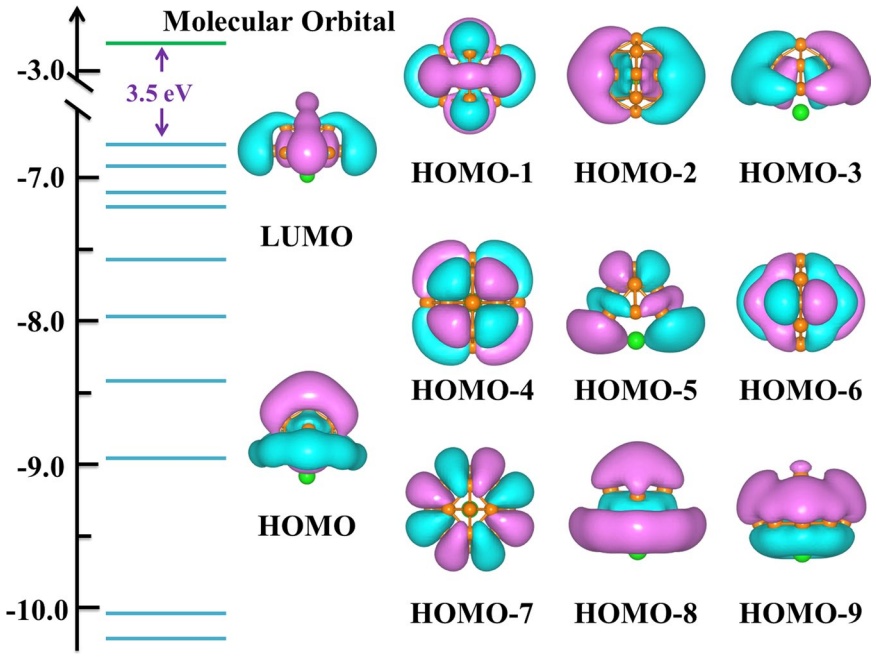

Figure 5. Visualized results of Molecular orbital and one-electron energy levels of the ground-state LiB_{13} cluster.

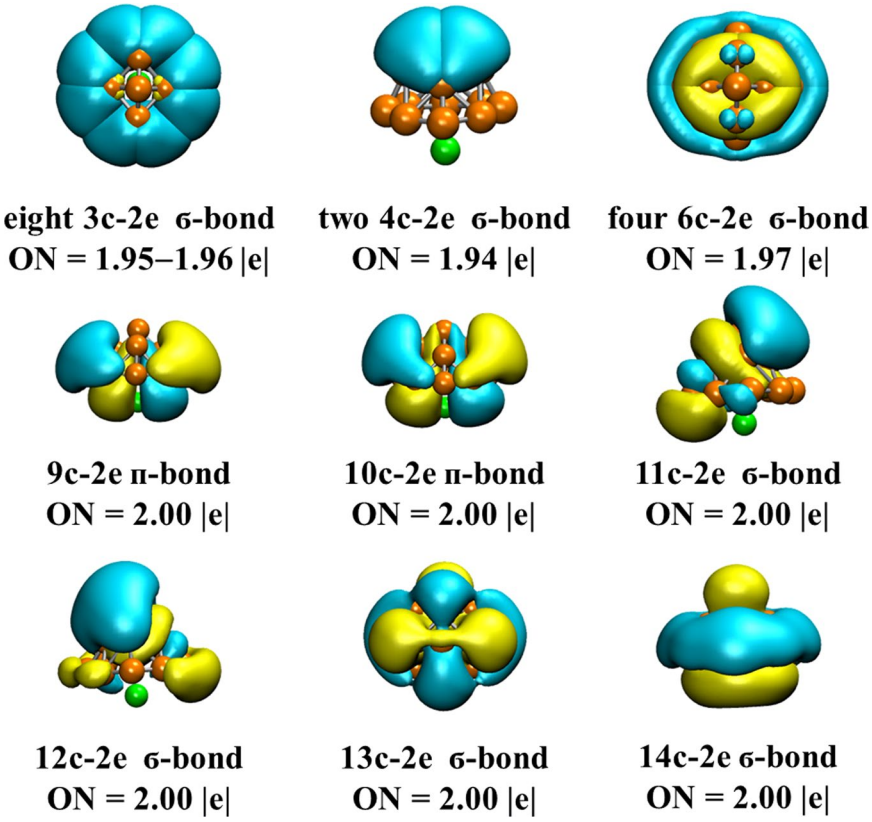

Figure 6. AdNDP (adaptive natural density partitioning) of the LiB_{13} cluster along with the ON (the occupation number).

analyses, it has been found that the 2p AOs of boron atoms have made necessary contributions for these molecular orbital. Meanwhile, stabilize of the LiB_{13} structure is attributed to the mutual effect between the Li atom and the B_{13} fragment.

To have a further understanding of the bonding properties of LiB_{13} cluster, the chemical bonding analysis by the means of AdNDP code was made. AdNDP algorithm describe the chemical bonding in terms of $nc-2e$ ($1 \leq n \leq$ the maximum number of atoms), which are obtained by partitioning the valence electron density matrix. The visualized results of LiB_{13} cluster together with their occupation number (ON) are presented in Fig. 6. All of the ONs approximately equal to the ideals values which lending credence to the AdNDP results we obtained. We divided these bonds into two categories: one work for the partial stability in the B_{13} shell and the other provide overall stability between the B_{13} moiety and the impurity atom Li. First, there are seventeen bonds on the B_{13} moiety and all of them are σ bond. The interactions of the B atoms in the peripheral B_8 ring and the middle B_4 ring are visualized by twelve σ bonds (eight 3c–2e bonds with ON = 1.95–1.96|e| and four 6c–2e bonds with ON = 1.97|e|). Meanwhile, the two 4c–2e σ bonds (ON = 1.94|e|) reveal the interactions between apical B atom and the four B atoms in the middle. Among the rest bonds, 11c–2e σ bonds, 12c–2e σ bonds and 13c–2e σ bonds, all the occupation numbers are 2.00|e|, also describe the B-B interaction in the B_{13} fragment. Then, there are three bonds for the integrity stability between the Li atom and the B_{13} shell and all of the three ON are 2.00|e|. Both of the 9c–2e π bonds and 10c–2e π bonds, formed by the 2 s orbital of Li atom the 2p orbital of B atoms, visualize the π mutual effect between the Li atom and part of the B_{13} shell. The connection between the entire B_{13} fragment and the Li atom is presented by the delocalized $14c-2e$ σ bond. Overall, both of the two groups of bonds earn substantial stabilization for the LiB_{13} cluster.

Conclusion

As a conclusion, we have presented a systematical research of the neutral and anionic lithium-doped boron clusters through CALYPSO structural search approach and DFT calculations. The lowest-energy geometric structures of $LiB_n^{0/-}$ ($n = 10$–20) clusters are determined. The evolution of the lowest-energy structures is that: half-surrounded structures for size n from 10 to 15 and quasi-planar or drum-type structures for the larger species ($n \geq 16$). The inherent stabilities have been analyzed by the average binding energy, second-order differences of energy and HOMO–LUMO energy gaps. A new tetrahedral-typed B_{13} ligand half-surround LiB_{13} cluster with high stability is identified. The molecular orbital and AdNDP analysis of the neutral LiB_{13} cluster suggest that B-B σ bonds in the B_{13} fragment combined with the strong interaction between B_{13} shell and Li atom stabilize the C_{2v} LiB_{13} cluster. This finding may provide guidance to future synthesis of boron-based nanomaterials.

Computational Details

Our structural search of neutral and anionic lithium-doped boron clusters are implemented by utilizing CALYPSO code[37–40]. The capability of this method has been successfully confirmed in structural prediction of several systems with only given the chemical composition[41–45]. We have followed fifty generations to achieve the global-minimum structures during the structural predictions. Every generation contains thirty structures. Thus, we can obtain about 1500 isomers for each cluster size *n*. The top fifty low-lying candidates are selected and re-optimized using the all-electron DFT theory via the Gaussian 09 package[46]. The optimization calculations are performed using the B3LYP functional[47,48] with 6–311 + G (d) basis set[49], which is chosen for both of the B and the Li atom. Multiple spin states up to sextet and quintet are fully involved for the structure optimization. Vibration frequencies calculations are performed to ensure all the isomers are global-minimum. The PES of the ground-state LiB_n^- clusters are calculated by means of the TD-DFT[50]. To further understanding the bonding mechanism of Li-doped boron clusters, the molecular orbital and AdNDP analyses[51] are calculated utilizing the Multiwfn 3.3.8 program package[52].

Data availability

The data in this manuscript is availability.

Received: 8 November 2019; Accepted: 2 January 2020;
Published online: 03 February 2020

References

1. Kroto, H. W., Heath, J. R., Obrien, S. C., Curl, R. F. & Smalley, R. E. C_{60}: Buckminsterfullerene. *Nature* **318**, 162–163 (1985).
2. Moreno, D. *et al.* B_{18}^{2-}: A quasi-planar bowl member of the Wankel motor family. *Chem. Commun.* **50**, 8140–8143 (2014).
3. Jalife, S. *et al.* Dynamical behavior of boron clusters. *Nanoscale* **8**, 17639–17644 (2016).
4. Saha, R. *et al.* A spinning umbrella: Carbon monoxide and dinitrogen bound MB_{12}^- clusters (M = Co, Rh, Ir). *J. Phys. Chem. A* **121**, 2971–2979 (2017).
5. Chen, X. *et al.* Lanthanides with unusually low oxidation states in the PrB_3^- and PrB_4^- boride clusters. *Inorg. Chem.* **58**, 411–418 (2019).
6. Chen, T. T., Li, W. L., Li, J. & Wang, L. S. $[La(\eta^x\text{-}B_x)La]^-$ (x = 7–9): A new class of inverse sandwich complexes. *Chem. Sci.* **10**, 2534–2542 (2019).
7. Cheung, L. F., Czekner, J., Kocheril, G. S. & Wang, L. S. High resolution photoelectron imaging of boron-bismuth binary clusters: Bi_2B_n (n = 2−4). *J. Chem. Phys.* **150**, 064304 (2019).
8. Pan, S. *et al.* Fluxional boron clusters: From theory to reality. *Acc. Chem. Res.* **52**, 2732–2744 (2019).
9. Vast, N. *et al.* Lattice dynamics of icosahedral α-boron under pressure. *Phys. Rev. Lett.* **78**, 693–696 (1997).
10. Fujimori, M. *et al.* Peculiar covalent bonds in α-rhombohedral boron. *Phys. Rev. Lett.* **82**, 4452–4455 (1999).
11. Martinez-Guajardo, G. *et al.* Dynamical behavior of borospherene: A nanobubble. *Sci. Rep.* **5**, 11287 (2015).
12. Zhai, H. J. *et al.* Observation of an all-boron fullerene. *Nat. Chem.* **6**, 727–731 (2014).
13. Piazza, Z. A. *et al.* Planar hexagonal B_{36} as a potential basis for extended single-atom layer boron sheets. *Nat. Commun.* **5**, 3113 (2014).
14. Chen, Q. *et al.* Quasi-planar aromatic B_{36} and B_{36}^- clusters: All-boron analogues of coronene. *Phys. Chem. Chem. Phys.* **16**, 18282–18287 (2014).
15. Wang, L. S. Photoelectron spectroscopy of size-selected boron clusters: From planar structures to borophenes and borospherenes. *Int. Rev. Phys. Chem.* **35**, 69–142 (2016).
16. Kiran, B. *et al.* Planarto-tubular structural transition in boron clusters: B_{20} as the embryo of single-walled boron nanotubes. *Proc. Natl. Acad. Sci. USA* **102**, 961–964 (2005).
17. Oger, E. *et al.* Boron cluster cations: Transition from planar to cylindrical structures. *Angew. Chem., Int. Ed.* **46**, 8503–8506 (2007).
18. Chen, Q. *et al.* Experimental and theoretical evidence of an axially chiral borospherene. *ACS Nano* **9**, 754–760 (2015).
19. Zhao, X. Y. *et al.* Cage-like B_{39}^+ clusters with the bonding pattern of σ+π double delocalization: new members of the borospherene family. *Phys. Chem. Chem. Phys.* **19**, 10998–11003 (2017).
20. Romanescu, C., Galeev, T. R., Li, W. L., Boldyrev, A. I. & Wang, L. S. Geometric and electronic factors in the rational design of transition-metal-centered boron molecular wheels. *J. Chem. Phys.* **138**, 134315 (2013).
21. Romanescu, C., Galeev, T. R., Li, W. L., Boldyrev, A. I. & Wang, L. S. Transition-metal-centered monocyclic boron wheel clusters ($M©B_n$): A new class of aromatic borometallic compounds. *Acc. Chem. Res.* **46**, 350–358 (2013).
22. Pan, S. *et al.* Boron nanowheel with an axle containing noble gas atoms: Viable noble gas bound $M©B_{10}^-$ clusters (M = Nb, Ta). *Chem. Eur. J.* **24**, 3590–3598 (2018).
23. Popov, I. A., Jian, T., Lopez, G. V., Boldyrev, A. I. & Wang, L. S. Cobalt- centred boron molecular drums with the highest coordination number in the CoB_{16}^- cluster. *Nat. Commun.* **6**, 8654 (2015).
24. Popov, I. A., Li, W. L., Piazza, Z. A., Boldyrev, A. I. & Wang, L. S. Complexes between planar boron clusters and transition metals: A photoelectron spectroscopy and ab initio study of CoB_{12}^- and RhB_{12}^-. *J. Phys. Chem. A* **118**, 8098–8105 (2014).
25. Liu, L. *et al.* Structure and bonding of IrB_{12}^-: converting a rigid boron B_{12} platelet to a Wankel motor. *RSC Adv.* **6**, 27177–27182 (2016).
26. Jian, T. *et al.* Competition between drum and quasi-planar structures in RhB_{18}^-: Motifs for metallo-boronanotubes and metallo-borophenes. *Chem. Sci.* **7**, 7020–7027 (2016).
27. Li, W. L. *et al.* Observation of a metal-centered B_2-Ta@B_{18}^- tubular molecular rotor and a perfect Ta@B_{20}^- boron drum with the record coordination number of twenty. *Chem. Commun.* **53**, 1587–1590 (2017).
28. Zhao, L. Q. *et al.* Effects of manganese doping on the structure evolution of small-sized boron clusters. *J. Phys.: Condens. Matter* **29**, 265401 (2017).
29. Galeev, T. R., Romanescu, C., Li, W. L., Wang, L. S. & Boldyrev, A. I. Valence isoelectronic substitution in the B_8^- and B_9^- molecular wheels by an Al dopant atom: Umbrella-like structures of AlB_7^- and AlB_8^-. *J. Chem. Phys.* **135**, 104301 (2011).
30. Chen, T. T. *et al.* PrB7−: A praseodymium-doped boron cluster with a Pr^{II} center coordinated by a doubly aromatic planar η^7-B_7^{3-} ligand. *Angew. Chem.* **135**, 1–6 (2017).
31. Kuznetsov, A. E. & Boldyrev, A. I. Theoretical evidence of aromaticity in X_3^- (X = B, Al, Ga) species. *Struct. Chem.* **13**, 141–148 (2002).
32. Alexandrova, A. N., Boldyrev, A. I., Zhai, H. J. & Wang, L. S. Photoelectron spectroscopy and ab initio study of the doubly antiaromatic B_6^{2-} dianion in the LiB_6^- cluster. *J. Chem. Phys.* **122**, 054313 (2005).
33. Tai, T. B. & Nguyen, M. T. Thermochemical properties, electronic structure and bonding of mixed lithium boron clusters (B_nLi, n = 1–8) and their anions. *Chem. Phys.* **375**, 25–45 (2010).

34. Dong, X. *et al*. Li_2B_{12} and Li_3B_{12}: prediction of the smallest tubular and cage-like Boron structures. *Angew. Chem. Int. Ed.* **57**, 4627–4631 (2018).
35. Liang, W. Y., Das, A., Dong, X. & Cui, Z. H. Lithium doped tubular structure in LiB_{20} and LiB_{20}^-: A viable global minimum. *Phys. Chem. Chem. Phys.* **20**, 16202–16208 (2018).
36. Zhai, H. J., Kiran, B., Li, J. & Wang, L. S. Hydrocarbon analogues of boron clusters—planarity, aromaticity and antiaromaticity. *Nat. Mater.* **2**, 827–833 (2003).
37. Lv, J., Wang, Y. C., Zhu, L. & Ma, Y. M. Particle-swarm structure prediction on clusters. *J. Chem. Phys.* **137**, 084104 (2012).
38. Wang, Y. C., Lv, J., Zhu, L. & Ma, Y. M. CALYPSO: A method for crystal structure prediction. *Comput. Phys. Commun.* **183**, 2063–2070 (2012).
39. Wang, Y. C., Lv, J., Zhu, L. & Ma, Y. M. Crystal structure prediction via particle-swarm optimization. *Phys. Rev. B: Condens. Matter Mater. Phys.* **82**, 094116 (2010).
40. Gao, B. *et al*. Interface structure Prediction via CALYPSO method. *Sci. Bull.* **64**, 301–309 (2019).
41. Li, Y. W., Hao, J., Liu, H. Y., Li, Y. L. & Ma, Y. M. The metallization and superconductivity of dense hydrogen sulfide. *J. Chem. Phys.* **140**, 174712 (2014).
42. Zhu, L., Liu, H. Y., Pickard, C. J., Zou, G. T. & Ma, Y. M. Reactions of xenon with iron and nickel are predicted in the earth's inner core. *Nat. Chem.* **6**, 644–648 (2014).
43. Zhu, L. *et al*. Substitutional alloy of Bi and Te at high pressure. *Phys. Rev. Lett.* **106**, 145501 (2011).
44. Lv, J., Wang, Y. C., Zhu, L. & Ma, Y. M. Predicted novel high-pressure phases of lithium. *Phys. Rev. Lett.* **106**, 015503 (2011).
45. Wang, H., Tse, J. S., Tanaka, K., Iitaka, T. & Ma, Y. M. Superconductive sodalite-like clathrate calcium hydride at high pressures. *Proc. Natl. Acad. Sci. USA* **109**, 6463–6466 (2012).
46. Frisch, M. J. *et al*. Gaussian 09 (Revision C.0), Gaussian, Inc., Wallingford, CT, (2009).
47. Becke, A. Density-functional thermochemistry. III. *The role of exact exchange. J. Chem. Phys.* **98**, 5648–5652 (1993).
48. Lee, C., Yang, W. & Parr, R. Development of the colic-salvetti correlation-energy formula into a functional of the electron density. *Phys. Rev. B: Condens. Matter Mater. Phys.* **37**, 785–789 (1988).
49. Krishnan, R., Binkley, J. S., Seeger, R. & Pople, J. A. Self-consistent molecular orbital methods. XX. *A basis set for correlated wave functions. J. Chem. Phys.* **72**, 650–654 (1980).
50. Casida, M. E., Jamorski, C., Casida, K. C. & Salahub, D. R. Molecular excitation energies to high-lying bound states from time-dependent density-functional response theory: Characterization and correction of the time-dependent local density approximation ionization threshold. *J. Chem. Phys.* **108**, 4439–4449 (1998).
51. Zubarev, D. Y. & Boldyrev, A. I. Developing paradigms of chemical bonding: adaptive natural density partitioning. *Phys. Chem. Chem. Phys.* **10**, 5207–5217 (2008).
52. Lu, T. & Chen, F. Multiwfn: a multifunctional wavefunction analyzer. *J. Comput. Chem.* **33**, 580–590 (2012).

Acknowledgements

This work is supported by the National Natural Science Foundation of China (Nos. 11574220 and 11874043).

Author contributions

X.Y.K. and C.L. conceived the idea. H.X.S. and C.L. performed the calculations. H.X.S. wrote the manuscript. All authors reviewed the manuscript.

Competing interests

The authors declare no competing interests.

Additional information

Supplementary information is available for this paper at https://doi.org/10.1038/s41598-020-57769-2.

Correspondence and requests for materials should be addressed to X.K. or C.L.

Reprints and permissions information is available at www.nature.com/reprints.

Publisher's note Springer Nature remains neutral with regard to jurisdictional claims in published maps and institutional affiliations.